Single-Molecule Interfacial Electron Transfer in Donor-Bridge-Nanoparticle Acceptor Complexes†

Shengye Jin,‡ Robert C. Snoeberger III,§ Abey Issac,‡ David Stockwell,‡ Victor S. Batista,*,§ and Tianquan Lian*,‡

Department of Chemistry, Emory University, Atlanta, Georgia, 3032 and Department of Chemistry, Yale University, New Haven, Connecticut, 06520-8107

Received: December 9, 2009; Revised Manuscript Received: February 19, 2010

Photoinduced interfacial electron transfer (IET) in sulforhodamine B (SRhB)-aminosilane-Tin oxide (SnO_2) nanoparticle donor−bridge−acceptor complexes has been studied on a single molecule and ensemble average level. On both SnO_2 and ZrO_2, the sum of single molecule fluorescence decays agree with the ensemble average results, suggesting complete sampling of molecules under single molecule conditions. Shorter fluorescence lifetime on SnO_2 than on ZrO_2 is observed and attributed to IET from SRhB to SnO_2. Single molecule lifetimes fluctuate with time and vary among different molecules, suggesting both static and dynamic IET heterogeneity in this system. Computational modeling of the complexes shows a distribution of molecular conformation, leading to a distribution of electronic coupling strengths and ET rates. It is likely that the conversion between these conformations led to the fluctuation of ET rate and fluorescence lifetime on the single molecule level.

Introduction

Interfacial electron transfer (IET) dynamics between molecular adsorbates and semiconductor nanoparticles and nanocrystalline thin films have been extensively studied in recent decades[1−6] due to its essential roles in solar cells,[7,8] photocatalysis,[5,9] and molecular electronics.[10] In most previous studies, ensemble averaged IET dynamics were measured by ultrafast transient absorption and time-resolved fluorescence spectroscopy.[11−28] The kinetics of charge injection from dye excited state to semiconductor nanoparticles and recombination were found to be in general nonsingle exponential, suggesting a heterogeneous distribution of IET rates. The nonexponential kinetics could result from static heterogeneities in energetics of the adsorbate and semiconductor and their electronic coupling as well as dynamic fluctuation of these quantities. These underlying distribution and fluctuation are masked in ensemble average measurements but can be revealed by single molecule (SM) spectroscopy.[29,30]

Single molecule fluorescence spectroscopy has been used to study electron transfer (ET) processes in molecules,[31,32] in conjugated polymers,[33] at interfaces[34−37] and in biological systems.[38−44] Studying ET process by single molecule fluorescence is still technically challenging, because it shortens the fluorescence lifetime and reduces fluorescence quantum yield of the dye molecules. As shown in Figure 1, the relationships of relevant deactivation processes and emission quantum yield can be described by eqs 1−3

$$\frac{1}{\tau} = k_r + k_{nr} = k_0 \tag{1}$$

$$\frac{1}{\tau'} = k_r + k_{nr} + k_{et} = k_0 + k_{et} \tag{2}$$

$$\Phi_0 = \frac{k_r}{k_0},\ \Phi_I = \frac{k_r}{k_0 + k_{et}} \tag{3}$$

where τ (τ') and $\Phi_0(\Phi_I)$ is the fluorescence lifetime and quantum yield, respectively, of the chromophore on inert (IET active) substrates, k_r and k_{nr} are the intrinsic radiative and nonradiative rate constants of the molecules, and k_{et} is IET rate constant.

Many ensemble averaged studies showed that IET from excited organic dyes (such as rhodamine and coumarin) that are directly attached to metal oxides (TiO_2, SnO_2, and ZnO) is often on the picosecond or faster time scale.[27,45−48] Assuming an intrinsic lifetime of 3 ns and quantum yield of ∼100%, the emission yield of molecules undergoing ultrafast IET (of 0.1−10 ps) can be estimated to be 0.003−0.3%, well below the

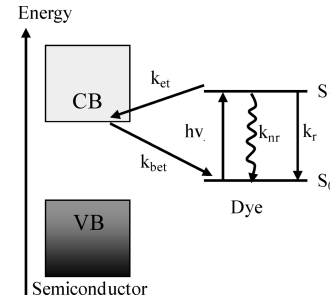

Figure 1. Schematic representation of photoinduced processes of dye molecules on semiconductor nanoparticles. k_r, radiative decay rate; k_{nr}, intrinsic nonradiative decay rate; k_{et}, IET rate from excited molecule to semiconductor; k_{bet}, back IET rate.

† Part of the "Michael R. Wasielewski Festschrift".

* To whom correspondence should be addressed. E-mail: (T.L.) tlian@emory.edu; (V.S.B.) victor.batista@yale.edu.

‡ Emory University.

§ Yale University.

10.1021/jp911662g
Published on Web 03/12/2010

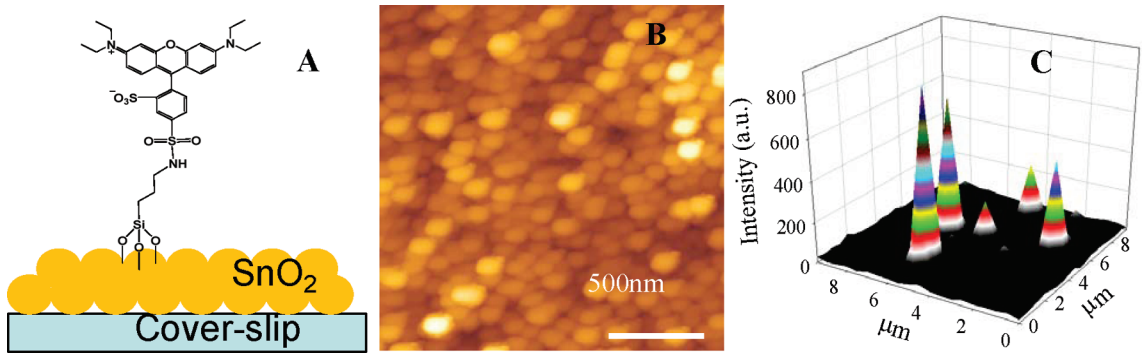

Figure 2. (A) A schematic structure of SRhB−silane−SnO_2, (B) AFM image of a SnO_2 nanocrystalline thin film, (C) a raster-scanned single molecule fluorescence image of Silane-SRhB-SnO_2 on a coverslip.

sensitivity of current SM spectroscopy technique. As a result, these IET events could not be directly observed. So far, there have been only a few published reports of single molecule IET.[34−37] In their pioneering work, Lu and Xie measured single molecule fluorescence lifetime of cresyl violet on ITO (Sn/In_2O_3).[34] They observed shorter fluorescence lifetimes on ITO than on glass and attributed it to IET from the excited dye to ITO. On the single molecule level, fluorescence decay was found to be single exponential, although there existed a distribution of lifetimes, suggesting a static inhomogeneous distribution of IET rates. Similar static heterogeneous distribution of ET rate was observed in our previous study of rhodamine B (RhB) on ATO.[36] We noted that the observed single molecule lifetimes are much longer than the ensemble averaged lifetimes due to incomplete sampling of molecules undergoing fast ET in the single molecule study. In a more recent study of coumarin on TiO_2, Lu and co-workers observed long (nanoseconds) SM fluorescence lifetimes as well as pronounced fluctuation of emission intensities.[37] The observed lifetime was thought to be much longer than the expected average electron injection time for this system. To account for the discrepancy between SM and ensemble averaged lifetimes, they proposed an intermittent IET activity model, according to which, the IET activity of molecules underwent significant fluctuation, changing between fast and slow (or none) injection states. In this model, most detected fluorescence photons originate from the slow injecting states. The fluorescence quantum yield of the fast injecting state was too low to be observed, and their presence was inferred from the fluctuation of emission intensity and the discrepancy between the single molecule and ensemble averaged fluorescence lifetimes. It remains unclear whether these observed single coumarin molecules on TiO_2 are representative of the whole ensemble, and if they are, why their behavior differs from those of RhB on ATO and creyl-violet on ITO.

In this paper, we describe a study of single molecule IET in a donor−bridge−acceptor system. Controlling interfacial ET rate by inserting spacers between the chromophore and semiconductor nanoparticles has been a subject of considerable interest.[49−54] It has been used as a convenient way to test the electronic coupling dependence of interfacial ET rates[50−52] and molecular conductances.[55] The spacer groups affect both the charge separation and recombination rates, offering a potential approach to optimize the efficiency of dye-sensitized solar cells.[54] The reduction of electron injection rate in the donor−bridge−acceptor complexes also decreases the degree of fluorescence quenching, allowing their observation under single molecule conditions. Furthermore, the introduction of the spacer units can introduce additional conformation flexibility in the molecules, leading to dynamical heterogeneity that is difficult to uncover by ensemble average measurements. As a proof of principle, we use an aminosilane bridge, whose amino group can be conjugated with organic dye molecules and silane group is coupled with semiconductor nanoparticle surfaces to construct interfacial donor−bridge−acceptor complexes (see Figure 2A). Sulforhodamine B chloride is chosen for its high quantum yield ($\Phi_f = \sim 0.6$),[56] high photostability, and the ability to conjugate with aminosilane. SnO_2 nanoparticles are used because IET from related RhB molecules have been reported in a previous ensemble average study using ultrafast spectroscopic techniques.[57] For this donor−bridge−acceptor system, we show that IET on a single molecule level can be studied. The sum of measured lifetimes of single molecules is consistent with the ensemble averaged results, indicating an unbiased sampling of all molecules. Single molecule study reveals that both static and dynamic heterogeneity contribute to the IET process in this system. The nature of molecular conformations that are responsible for the observed heterogeneity was investigated by computer simulation of the system.

Experimental Section

Synthesis of Silane-Conjugated Sulforhodamine B. Silane conjugated sulforhodamine B (SRhB−silane) was synthesized through the reaction between sulforhodamine B acid chloride (Fluka, referred as SRhB) and 3-aminopropyltrimethoxysilane (referred as aminosilane, 97%, from Aldrich) according to a literature procedure.[58] SRhB (0.012 g) and 0.01 g of 4-dimethylaminopyridine were added into 3 mL of dry pyridine (Sigma, 99%), and after stirring for 30 min 10 μL of aminosilane was injected and allowed to react for 3 h. The product was purified by eluting through a silica gel column (100−200 mesh, 60 Å, Sigma-Aldrich, eluent: 5/1 chloroform/methanol solvent). The measured mass/charge ratio was 762.29127, consistent with the calculated value of 762.29088 for $[C_{36}H_{51}O_9N_3S_2Si + H]^+$. Compared to SRhB, the UV−vis absorption peak of SRhB−silane was red shifted by 7 nm (result not shown), and its fluorescence lifetime in ethanol solution was unchanged (3.1 ns, result not shown).

Preparation of SnO_2 and ZrO_2 Nanoparticle Films. SnO_2 nanoparticles were synthesized according to a published procedure.[59] Eighty-five millimoles (~10 mL) of $SnCl_4$ (99.9%, Aldrich) was injected into 20 mL of HCl (37 wt %) by syringe and dispersed by sonication for at least 30 min. The resulting solution was added dropwise into 500 mL of water under rapid stirring at 0 °C. After stirring for an additional 30 min, aqueous ammonia (25%) was added to the solution until a pH value of 3.5−4.0 was reached. The solution was kept in the dark for over 12 h to allow the precipitation of SnO_2 nanoparticles. The white precipitate was washed at least 3 times with distilled water

and then suspended in 300 mL of water whose pH was adjusted to 9.5−10. The suspension was stirred vigorously overnight and dialyzed against ∼10 L of water at pH 10 for at least two days. The resulting transparent SnO_2 colloid was then refluxed for 4 h. One hundred fifty milliliters of this colloid was poured into an autoclave and heated first at 150 °C for 1 h and then at 270 °C for 16 h. Solid SnO_2 nanoparticles were obtained by rotary evaporation of the solution under vacuum. SnO_2 nanoparticle water solution (0.01 g/mL) was spin coated on cover glass slides (Fisher Scientific) and sintered at 550 °C for 2.5 h to produce SnO_2 nanocrystalline thin films. An atomic force microscopy (AFM) image of a SnO_2 nanocrystalline thin film is shown in Figure 2B.

ZrO_2 powder (2 g, from Degussa Corporation) was ground in a mortar with distilled water (4 mL), acetylacetone (10 μL), and 5 drops of Triton X-100 to break up the aggregate into a dispersed paste. The paste was washed several times by water. A final diluted ZrO_2 nanoparticle water solution (∼0.01 g/mL) was spin coated on glass coverslips. The films were then sintered at 550 °C for 2.5 h.

Donor−Bridge−Acceptor Preparation. A drop (∼20 μL) of SRhB−silane water (Millipore, 18.2 MΩ/cm) solution was dropped on the surfaces of substrates (SnO_2 or ZrO_2 nanocrystalline thin films, or glass coverslip). After drying in the dark, the substrates were heated at 120 °C for 10 min and then washed with water to remove unreacted SRhB−silane molecules. Here we refer to SRhB−silane immobilized on different substrates as SRhB−silane−SnO_2 (or ZrO_2, Glass). The concentrations of the SRhB−silane solutions used were $\sim10^{-4}$, $\sim10^{-8}$, $\sim10^{-11}-10^{-12}$ M for the samples for transient absorption, ensemble average fluorescence, and single molecule fluorescence measurements, respectively. Fluorescence (single molecule and ensemble averaged) and transient absorption measurements were performed with nanocrystalline thin films prepared on glass coverslip and sapphire windows respectively.

Single Molecule Fluorescence. Excitation beam at 500 nm was generated by frequency doubling in a BBO crystal of the 1000 nm output (100 fs, 80 MHz repetition rate) from a mode-locked Ti:Sapphire laser (Tsunami oscillator pumped by 10 W Millennia Pro, Spectra-Physics). The laser beam was focused through an objective (100× N.A 1.4, oil immersion, Olympus) onto the samples placed on a piezo scanner (Mad City Laboratories). All wide-field-illuminated fluorescence images were obtained using a CCD camera (Roper Scientific, VersArray 512B) under the same excitation condition (excitation wavelength $\lambda_{exc} = 500$ nm, average excitation power density $P_{exc} = 400$ W/cm^2).

Single-molecule trajectories were recorded by focusing the excitation beam (∼200 nW) down to a diffraction-limited spot (∼300 nm diameter) on the sample and detecting epi-fluorescence from the sample by an avalanche photodiode (APD, EG & G model SPCM-14). The APD output was analyzed by a time-correlated single photon counting (TCSPC) board (Becker & Hickel SPC 600) operating in the photon-stamping mode.[37,38] The fluorescence intensity trajectory was recorded until the molecule underwent irreversible photobleach. The lifetime trajectory of single molecules was created by constructing the delay time histogram of photons with a 2 s bin time and 0.5 s step size. The background photons for single molecules were collected after the photobleach of the molecules, and the average background decays within 2 s bin time were then calculated and subtracted from the single molecule fluorescence decay curves. The instrument response function of the fluorescence lifetime measurement has a full-width-at-half-maximum (fwhm) of 500 ps.

Ensemble Fluorescence Decay and Ultrafast Transient Absorption Measurements. Ensemble averaged fluorescence was measured in the same setup as single molecule fluorescence using a sample with 10 000 times higher SRhB−silane concentration. The samples were continuously scanned during the measurement to average over a wide area and to avoid photodegradation.

The visible spectrometer used for ultrafast transient absorption experiments was based on a regeneratively amplified Ti:Sapphire laser system (Coherent Legend, 800 nm, 150 fs, 2.5 mJ/pulse, 1 kHz repetition rate) and an optical parametric amplifier (OPA). Pump pulses at 532 nm were generated by sum frequency mixing of the signal outputs (80 μJ) of an IR-OPA (Clark-MXR, pumped with 1 mJ of 800 nm pulse) and the 800 nm beam (∼100 μJ) in a BBO crystal. The diameter and energy of the 532 nm pulse were 300 μm and 25 nJ/pulse, respectively. The visible probe (white light continuum, 430 to 750 nm) was generated by attenuating and focusing ∼10 μJ of the 800 nm pulse into a 2 mm thick sapphire window. The probe was focused on the sample using protected Al parabolic reflectors to a spot size of 150 μm at 532 nm. After the sample, the probe was focused into a fiber-coupled spectrometer (Ocean Optics USB2000, 2048 pixel CCD, ∼0.25 nm/pixel readout) and detected at a frequency of 10 Hz. The pump pulses were chopped by a synchronized chopper to the same frequency. Zero time delay and the instrument response function were obtained with the instantaneous ground state bleach at 550 nm of RhB in ethanol solution. During the data collection, samples were constantly translated at a speed of 5 mm/min to avoid photodegradation.

Computational Methods and Structural Models. This section describes the computational models and methods applied for calculations of fluorescence lifetimes of sulforhodamine B−aminosilane−SnO_2 nanoparticle donor−bridge−acceptor complexes. Fluorescence lifetimes τ' were obtained, according to eq 2, by computing the intrinsic decay times τ ($=1/k_0$) and electron injection times τ_{et} ($=1/k_{et}$) for an ensemble of configurations of the system at thermal equilibrium. The quantum yield Φ_I, obtained from τ and τ_{et} according to eq 3, determines the statistical weight of each configuration to the overall distribution of fluorescence lifetimes τ'. Therefore, configurations with short τ_{et} have a small quantum yield and contribute little to the overall distribution of fluorescence times since they are most likely to undergo interfacial electron transfer and suppress fluorescence.

The intrinsic decay time τ is obtained, according to eq 1, from the radiative lifetime τ_r ($=1/k_r$) and the intramolecular nonradiative decay time $\tau_{nr} = \tau_{sol}/(1 - \Phi)$. The latter, $\tau_{nr} = 7.7$ ns, is estimated from the experimental fluorescence lifetime $\tau_{sol} = 3.1$ ns for SRhB in ethanol and the reported fluorescence quantum yield of RhB in ethanol $\Phi = 0.6$.[56] The radiative decay times τ_r on surfaces are estimated as follows

$$\tau_r = \tau_\infty \left(\frac{L_\parallel(z)}{L_\infty} \sin^2(\theta_e) + \frac{L_\perp(z)}{L_\infty} \cos^2(\theta_e) \right)^{-1} \qquad (4)$$

by taking into account the effect of the dielectric interface[60] on the radiative lifetime $\tau_\infty = 11.9$ ns of SRhB in water (i.e., infinitely far from the dielectric interface). The value of τ_∞ was set to reproduce the experimental fluorescence lifetime of SRhB on a semiconductor surface where there is no IET (e.g., ZrO_2).

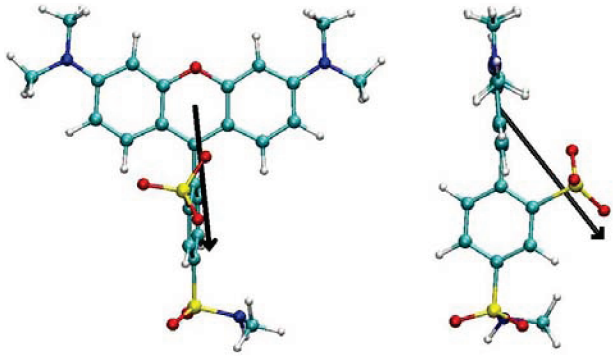

Figure 3. Orientation of the $S_1 \leftarrow S_0$ transition dipole moment (black arrow) of SRhB−silane obtained at the TDDFT-B3LYP/6-31G(d) level of theory. Color key: O (red), C (light blue), N (blue), and H (white).

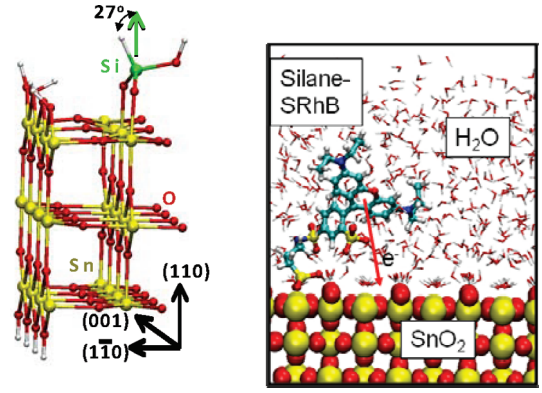

Figure 4. (Right) Attachment of the silane linker to the SnO_2 surface as described at the DFT PW91 level of theory; and (Left) Snapshot of SRhB−silane on the (110) surface of SnO_2 exposed to room-temperature humidity conditions. Color key: O (red), C (light blue), N (blue), H (white), Si (light yellow), and Sn (gray yellow).

The ratios of radiative power perpendicular and parallel to the interface $L_{\|}/L_{\infty}$ and $L_{\perp}/L_{\infty}$, introduced by eq 4, depend on the difference of refractive indices of the media at the interface.[61] Our calculations for water/SnO_2 and water/ZrO_2 interfaces are based on refractive indices 1.333, 2.006, and 2.130 for water, SnO_2 and ZrO_2, respectively.[62] These ratios also depend on the distance z (∼1 nm) of the adsorbate chromophore from the surface, although in practice they are approximated to zeroth order in z, as follows

$$\frac{L(z)}{L_{\infty}} = l_0 + l_1\left(\frac{4\pi z}{\lambda_1}\right) + \ldots \approx l_0 \qquad (5)$$

since the wavelength of the incident light λ_1 (∼500 nm) ≫ z. According to eqs 4 and 5, the intrinsic lifetimes for molecules with transition dipole moments parallel and perpendicular to the semiconductor surface are 4.1 and 3.1 ns for SnO_2, and 3.9 and 2.9 ns for ZrO_2, respectively.

Computing the radiative decay time τ_r, according to eq 4, also requires the angle θ_e between the emission dipole and the surface normal for each representative configuration. Transition dipole moments are estimated according to density functional theory (DFT) B3LYP[63]/6-31G(d),[64,65] as implemented in the Gaussian 03 suite of computational chemistry software,[74] from computations of vertical transitions at the time-dependent (TD) DFT[66−68] level of theory for the SRhB−silane adsorbates with the aminosilane linker truncated as a methyl group. Figure 3 shows the orientation of the $S_1 \leftarrow S_0$ transition dipole moment with respect to the molecular structure. In the plane of the molecule, the transition dipole moment points toward the aminosilane linker (Figure 3, left panel) while in the direction normal to the molecular plane, the transition dipole moment points toward the sulfonate group (Figure 3, right panel). The orientation of the transition dipole therefore can be correlated with the orientation of the sulfonate group. For example, when $\theta_e > 90°$ the sulfonate group is pointing toward the surface, and when $\theta_e < 90°$ the sulfonate group is pointing away from the surface. Furthermore, when $\theta_e \sim 180°$ (as oriented in Figure 2), the sulfonate group is below the three conjugated rings relative to the surface, while $\theta_e \sim 0°$ leaves the three conjugated rings below the sulfonate group and in close contact with the surface.

An ensemble of representative configurations was generated by molecular dynamics (MD) simulations at 300 K to sample the distribution of angles θ_e generated by thermal fluctuations, due to the conformational flexibility of the aminosilane linker covalently attaching SRhB to the semiconductor surface. The simulations were performed by using the molecular dynamics package NAMD,[69] including a 2 nm thick layer of water molecules hydrating the surface as shown in Figure 4 to mimic the SnO_2 samples studied in the experiments that were exposed to air. Under these conditions the oxide surfaces were hydrated by layers of water molecules.[70,71] All MD simulations were subject to the constraint of fixed nuclear coordinates for the SnO_2 units and the siloxane linker, as in the DFT minimum energy configuration. SRhB−silane was described according to the Amber[72] molecular mechanics force field with atomic charges parametrized to fit the ab initio electrostatic potential obtained from DFT-B3LYP/6-31G(d) calculations. The SnO_2 charges and interaction parameters were obtained from the work of Bandura et al.[73]

The attachment of the aminosilane linker to the SnO_2 surface (110) was modeled at the DFT level. The surface was represented by a periodic slab composed of 108 [SnO_2] units (i.e., 3 layers of Sn^{4+} ions and 9 layers of O^{2-} ions) with a vacuum spacer of 10 Å along the direction of the surface normal. The surface bridging O^{2-} ions were capped with hydrogen atoms and the silane molecule was adsorbed in a bridging mode between two penta-coordinated Sn^{4+} ions on the surface (see Figure 4). The DFT calculations were performed using the Vienna Ab initio Simulation Package (VASP),[74−76] employing Vanderbilt ultrasoft pseudopotentials,[77] a planewave basis truncated at 400 eV and electron exchange and correlation described using the PW91[78] functional. A 5 × 1 × 1 Monkhorst-Pack k-point sampling was used to integrate over the Brillouin zone.

Electron transfer times $\tau_{et} = \hbar/\gamma$ were computed for each representative configuration generated to determine the distribution of angles θ_e. The energy broadening γ of the initially populated electronic state in the adsorbate molecule was computed, as follows[79]

$$\gamma = \sum_i p_i |E_d - \varepsilon_i| \qquad (6)$$

with p_i the population of the i^{th} orbital with energy ε_i and

$$E_d = \sum_i p_i \varepsilon_i \qquad (7)$$

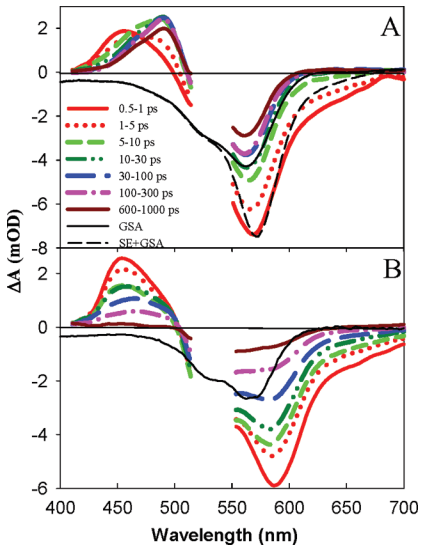

Figure 5. Transient absorption spectra of (A) SRhB−SnO_2 and (B) SRhB−silane−SnO_2 recorded at indicated delay time following 532 nm excitation. Also plotted along the negative vertical axis is the ground-state absorption (GSA) of SRhB−SnO_2 and SRhB−silane−SnO_2 (solid black lines), as well as the sum of GSA and static emission of SRhB in ethanol (dashed black line). At early delay times, the transient spectra consist of the bleach of ground-state absorption (∼560 nm), stimulated emission (∼567 nm) and excited state absorption (∼460 nm) in both (A) and (B). In (A) the decay of excited state (absorption and stimulated emission) leads to the formation of oxidized SRhB (∼494 nm) and long-lived ground state bleach, indicating the presence of IET.

the energy of the initial state. The energies ε_i were obtained from the extended Hückel Hamiltonian of the SRhB−silane−SnO_2 system,[80] assuming that the surrounding solvent has little influence on the coupling between the adsorbate SRhB−silane and the SnO_2 surface. We note, however, that the estimation of IET times based on eq 6, is most accurate for rather short IET times (e.g., <100 fs) and is less accurate for longer IET times since γ can only be resolved to a width comparable to the energy spacing (∼0.005 eV) between electronic states of the conduction band of the model supercell.

Results and Discussions

Ensemble Average ET Dynamics. The ensemble averaged electron injection dynamics from excited RhB molecules to SnO_2 nanocrystalline thin films have been investigated recently by transient absorption in the visible and mid-IR.[45] Electron transfer process was monitored by the decay of RhB excited state absorption and stimulated emission and the formation of RhB cation and injected electrons in SnO_2. Similar transient absorption spectra of SRhB sensitized SnO_2 nanocrystalline thin films after 532 nm excitation are shown in Figure 5A. The observed features can be assigned following those for RhB, since the UV−vis absorption spectrum of SRhB is only slightly red shifted (∼10 nm) from RhB.[45] The spectra after 10 ps consist of a bleach of ground state absorption that agrees well with the static absorption spectrum (solid line), and a peak at 494 nm that can assigned to the absorption of oxidized SRhB ($SRhB^+$).[45] In the first 10 ps, the transient spectra show a decay of the SRhB excited state (absorption at ∼460 nm and stimulated emission at ∼657 nm) and the formation of $SRhB^+$ (∼494 nm), indicating ET from excited SRhB to SnO_2 on this time scale. The decay of the signal at ∼560 nm in the first 10 ps is attributed mainly to the decrease of stimulated emission (550−700 nm), which

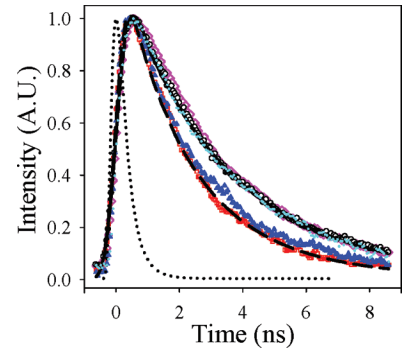

Figure 6. Ensemble average fluorescence decays of SRhB−silane on glass (pink open diamonds), ZrO_2 (black open circles), and SnO_2 (red open squares), and the instrument response function of these measurements (dotted line). Multiexponential fits for the data on ZrO_2 (black solid line) and SnO_2 (black dashed line) are also shown. Averaged fluorescence decays constructed from the sum of single SRhB−silane decays on SnO_2 (blue filled triangles) and on ZrO_2 (cyan filled diamonds) are also shown.

overlaps with the ground state bleach at this wavelength. This assignment is supported by a qualitative agreement between the transient spectra at 0.5−1 ps with a simulated spectrum consisting of the bleach of ground state absorption (with the same amplitude as the signal at 10−30 ps) and stimulated emission (approximated by the static emission of SRhB in ethanol). On the 10−1000 ps time scale, both the amplitudes of $SRhB^+$ absorption and ground state bleach decrease slightly which can be attributed to the recombination of the $SRhB^+$ with injected electrons to reform SRhB molecules in the ground state.

Photoinduced ET from SRhB to SnO_2 should also occur in the donor−bridge−acceptor complex, although the rate is expected to be significantly slower due to the presence of the aminosilane bridge. The transient absorption spectra of SRhB−silane−SnO_2 are shown in Figure 5B. In this case, the decays of excited state absorption (∼460 nm) and stimulated emission (550−700 nm) did not lead to the formation of $SRhB^+$ (absorption at ∼494 nm) on the same time scale. Instead, they lead to regeneration of the ground state as indicated by the recovery of the ground state bleach. The presence of an isosbestic point at 510 nm further indicates that the transient spectra in this region consist of two species (excited absorption at 460 nm and ground state bleach) that are formed instantaneously and decay with the same kinetics. The excited state decay occurred in a few hundreds of picoseconds, much shorter than the 3 ns excited state lifetime of isolated SRhB in solution. This decay is attributed to the quenching between excited dye molecules on SnO_2 films, similar to that observed for RhB/ZrO_2 in which ET from excited RhB to ZrO_2 is not energetically allowed.[45] Under these conditions, the interfacial ET rate is slower than the quenching rate among excited adsorbate molecules (a few hundred picoseconds). Unfortunately, the sensitivity of the transient absorption measurement is not sufficient to carry out studies under lower excitation power and/or dye coverage, at which the self-quenching effect can be reduced.

To reduce chromophore self-quenching effect, we measured ensemble averaged ET dynamics by TCSPC, which can be performed at much lower dye coverage and excitation power. For these measurements, we prepared SRhB−silane−SnO_2 (or ZrO_2 or glass) with chromophore concentration as low as $\sim 10^{-8}$ M (10 000 times lower than the transient absorption study). As shown in Figure 6, the fluorescence decays of SRhB−silane−ZrO_2 and SRhB−silane−glass are similar, whereas it is faster

TABLE 1: Bi-Exponential Fitting Parameter for Fluorescence Decay of SRhB−silane on ZrO_2 and SnO_2[a]

	a_1	τ_1 (ns)	a_2	τ_2 (ns)	τ_{ave} (ns)
SRhB−silane−ZrO_2	0.45 ± 0.02[b]	4.3 ± 0.2	0.55 ± 0.02	2.7 ± 0.1	3.4 ± 0.4
SRhB−silane−SnO_2	0.36 ± 0.01	3.7 ± 0.2	0.64 ± 0.02	1.8 ± 0.04	2.5 ± 0.2

[a] a_i and τ_i are amplitudes and time constants of i^{th} (=1,2) exponents, and τ_{ave} is the amplitude weighted average time constant, as defined in eq 9. [b] Errors indicates one standard deviation.

in SRhB−silane−SnO_2. ET from SRhB to ZrO_2 is not energetically allowed because the conduction band edge position of ZrO_2 is higher than the oxidation potential of excited SRhB. Because the refractive index and morphology of ZrO_2 films are similar to SnO_2, the effects of the dielectric constant on the radiative lifetime of the molecules on these surfaces are similar, which will be detailed later in the computation result section.[60,62] Therefore, we attribute the faster fluorescence decay on SnO_2 to IET from SRhB−silane to SnO_2 nanoparticles.

The fluorescence decays for SRhB−silane−ZrO_2 and SRhB−silane−SnO_2 can be well fit by biexponential kinetics, $S(t)$

$$S(t) = a_1 e^{-t/\tau_1} + a_2 e^{-t/\tau_2} \quad (8)$$

where a_i and τ_i are amplitudes and time constants of the i^{th} (=1,2) exponential component. From these fitting parameters, the amplitude weighted average time constant, τ_{ave} can be calculated

$$\tau_{ave} = \frac{a_1\tau_1 + a_2\tau_2}{a_1 + a_2} \quad (9)$$

These fitting parameters and the average time constants are listed in Table 1. As indicated by the biexponential kinetics and confirmed by the single molecule studies to be shown below, there is a distribution of k_0 on ET inactive substrates, which prevents an accurate determination of ET rate by comparing lifetimes on ET active and inactive substrate according to eqs 1 and 2. As a rough estimate, we assumed that $1/k_0 = 3.2$ ns, the average lifetime on ZrO_2, and from the average lifetime on SnO_2, we calculated an average ET time of 11 ns. The ET time in SRhB−SnO_2 is about a few picoseconds. For the SRhB−silane−SnO_2 complex, there are 9 bonds separating the conjugated region of the chromophore and the SnO_2. Assuming an exponential decay constant of roughly 1 per bond,[81] we estimate an ET time in this donor−bridge−acceptor system of ~10 ns, similar to the average IET time estimated from the measured fluorescence lifetimes.

Wide-Field Imaging of Single Molecules. To confirm that the ET activity is also present under single molecule conditions, we compared samples of SRhB on SnO_2 and on glass prepared with similar number densities of SRhB molecules. As shown by the wide-field-illuminated fluorescence images of these samples, the number of observable single molecules on SnO_2 (Figure 7B) is much less than that on glass (Figure 7A). This comparison confirms that on SnO_2, fluorescence of SRhB is quenched due to electron transfer on the picosecond time scale. It is interesting to note that fluorescence lifetimes of the few observable molecules are around 3 ns, which is similar to the lifetime on the glass surface. Under these conditions, the molecules detected by single molecule fluorescence measurements account for a few percent of the excited state population, and these molecules either inject electrons at a slow rate

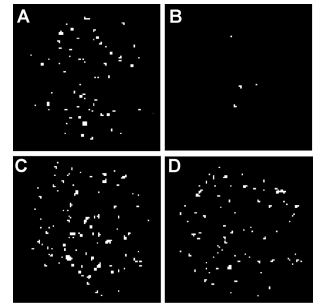

Figure 7. Wide-field-illuminated fluorescence images (25 μm × 25 μm) of similar numbers of single SRhB molecules dropped on glass (A) and a SnO_2 film (B), and similar numbers of single SRhB−silane molecules immobilized on ZrO_2 (C) and SnO_2 (D) nanocrystalline thin films. All images are obtained under the same condition ($\lambda_{exc.}$: 500 nm; $P_{exc.}$ = 400 W/cm^2).

(≪1/(3 ns)) or do not undergo IET at all. Similar observation has been reported before for RhB molecules on Sb−SnO_2 (ATO).[36]

The long-fluorescence lifetime (slow ET rate) of the SRhB−silane−SnO_2 complexes enable their study by single molecule fluorescence spectroscopy. This is confirmed by comparing the wide-field-illuminated fluorescence images of single SRhB−silane molecules immobilized on ZrO_2 (Figure 7C) and SnO_2 (Figure 7D) films. These samples were prepared with similar number densities of SRhB−silane molecules. Indeed, similar numbers of single molecules were observed on these substrates, suggesting the sampling of most molecules on ET active substrates. Furthermore, as shown in Figure 6, the sums of the fluorescence decays of 103 and 68 single SRhB−silane molecules on SnO_2 and ZrO_2, respectively, are similar to the ensemble averaged fluorescence decays on these substrates, confirming a near complete sampling of all molecules under single molecule conditions. Therefore, the single molecule ET dynamics to be discussed below represents the dynamics of the whole ensemble.

Single Molecule Dynamics on ZrO_2. The nonsingle exponential fluorescence decay of SRhB−silane on ZrO_2 and SnO_2 suggests inhomogeneous distributions of lifetimes. To quantify these distributions and investigate their origins, we have measured the fluorescence lifetime of single molecules. For each single molecule, the trajectory of fluorescence intensity and lifetime are recorded. The intensity was calculated with bin time of 0.1 s and lifetime trajectory was obtained with 2 s bin time and 0.5 s step size.

We first discuss the result of 68 single molecules on ZrO_2 where ET is not expected. Figure 8 shows two typical single molecule fluorescence and lifetime trajectories on ZrO_2 as well as their corresponding lifetime histograms. The lifetime histograms were constructed with a step size of 200 ps, which is the accuracy of lifetime measurement in this study. Shown in Figure 8F is a plot of chi-square of single exponential fit as a function of lifetime for a total of ~800 photons for a single SRhB−silane−SnO_2. This corresponds to the lowest number of total photons in a 2 s window and represents the largest uncertainty in lifetime determination. The change in χ^2 increases by ~20% when lifetime deviates from the best fit value by ~200

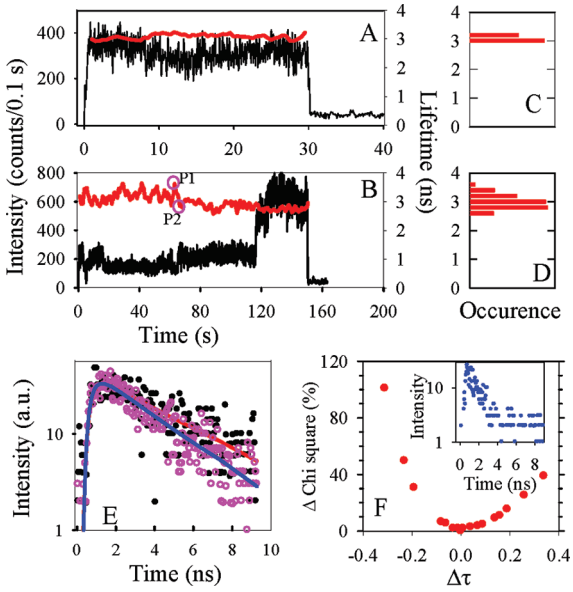

Figure 8. (A,B) Typical fluorescence intensity (black) and lifetime (red) trajectories of two single SRhB−silane molecules on ZrO_2, and (C,D) their corresponding lifetime histogram. (E) The fluorescence decay curves of the points P1 and P2 in C. (F) Change of χ^2 of single exponential fit to a fluorescence decay curve (shown in inset) as a function of lifetime for SRhB−silane−SnO_2.

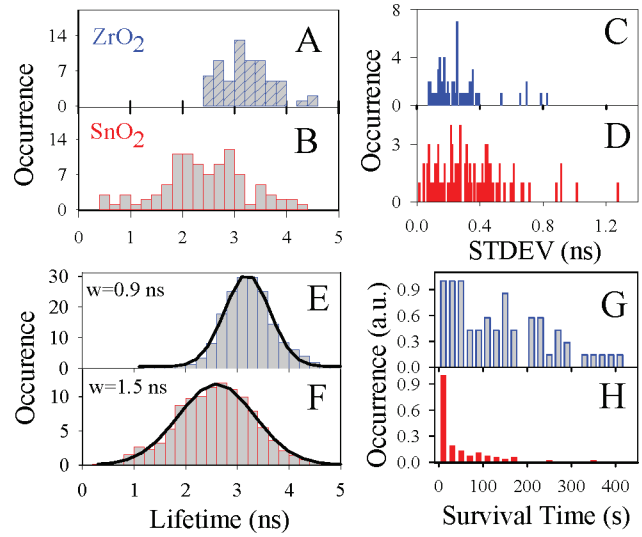

Figure 9. Histograms of average single molecule fluorescence lifetime (A and B), standard deviations (C and D), total lifetime distribution (E and F), and survival times (G and H) for SRhB−silane on ZrO_2 and SnO_2, respectively. The total lifetime distribution histograms are the sum of lifetime histrograms of all single molecules.

ps. As an example, we compare in Figure 8E the fluorescence decay curve for two points (P1 and P2) in the lifetime trajectory shown in Figure 8C. The best fit lifetime values of these points are 3.3 and 2.8 ns respectively, and their decay curves can be differentiated.

From each single molecule fluorescence lifetime histogram, we compute the average (τ^s_{ave}) and standard deviation (σ) of lifetimes

$$\tau^s_{ave} = \frac{\sum_i p_i \tau_i}{\sum_i p_i}$$
$$\sigma = \sqrt{\frac{\sum_i p_i (\tau_i - \tau_{ave})^2}{(\sum_i p_i - 1)}} \qquad (10)$$

where p_i, and τ_i are the occurrence and lifetime of the lifetime histogram for each molecule. As shown in Figure 9E, the average lifetimes of single molecules vary from 2.4 to 4.6 ns with a peak at 3.2 ns. Most (90%) single molecule trajectories show a small fluctuation of lifetimes around their average values ($\sigma < 0.4$ ns). As indicated by the individual trajectories (see for example, Figure 8B), the lifetime fluctuation appears to have no correlation with change in fluorescence intensity.

Because lifetime fluctuates over the duration of measurement for each molecule, the distribution of average lifetime does not adequately describe the ensemble distribution of lifetime. Instead, we added up the lifetime histograms of all single molecules. The resulting total histogram shown in Figure 9E should reflect the lifetime distribution of the whole ensemble. The distribution can be well described by a Gaussian function with a center at 3.3 ns and a fwhm of 0.9 ns. It is worth noting that although the ensemble average fluorescence decay of this sample can be fit phenomenologically by biexponential decay (see Figure 6), this fit does not reveal the underlining heterogeneous distributions. Through the study of single molecules, these distributions can be revealed.

Single molecule lifetimes on an ET inactive substrate depend on radiative and nonradiative rates. The nonradiative decay rate of RhB is determined by polarity and rigidity of the medium because of the presence of twisted intramolecular charge-transfer (TICT) excited states.[82,83] Its quantum yield was about 1 in a rigid environment and radiative decay time was about 5 ns in alcohols.[56] An increase in the nonradiative decay rate will lead to a decrease in the fluorescence quantum yield and lifetime. As shown in Figure 8, there is no correlation between the fluctuations in lifetime and intensity. For example, the molecule in Figure 8B shows a sudden change of fluorescence intensity at ~115 s but with a negligible change of fluorescence lifetime. Therefore, the observed distribution and fluctuation of lifetimes cannot be attributed to a fluctuation in nonradiative decay rate. For a fluorescence molecule at an interface, its radiative lifetime depends on the refractive index of the media and the orientation of the molecule relative to the interface normal.[60,84] A distribution of single molecule lifetimes on glass due to variation of orientation has been observed in previous studies.[36,60] We attribute the observed lifetime distribution to the distribution and fluctuation of the orientation of SRhB−silane molecules relative to surface normal. This orientation change may increase or decrease the emission intensity, depending on how it affects the projection of the transition dipole relative to the polarization of the linearly polarized excitation pulse. As we will discuss below, the presence of the bridge introduces conformation flexibility in the donor−bridge−acceptor system studied here. In addition to the fluctuation of lifetimes, the single molecule trajectories on ZrO_2 (such as those shown in Figure 8) also exhibit variation of fluorescence intensity. These intensity fluctuations are similar to other single molecules on non-ET active substrates and have been attributed to spectral diffusion and formation of nonemissive states.[29,30,85−87]

Single Molecules on SnO_2. Single SRhB−silane molecules (103) on SnO_2 were studied by single molecule fluorescence spectroscopy. Fluorescence intensity and lifetime trajectory were constructed for each single molecule, except for nine of them,

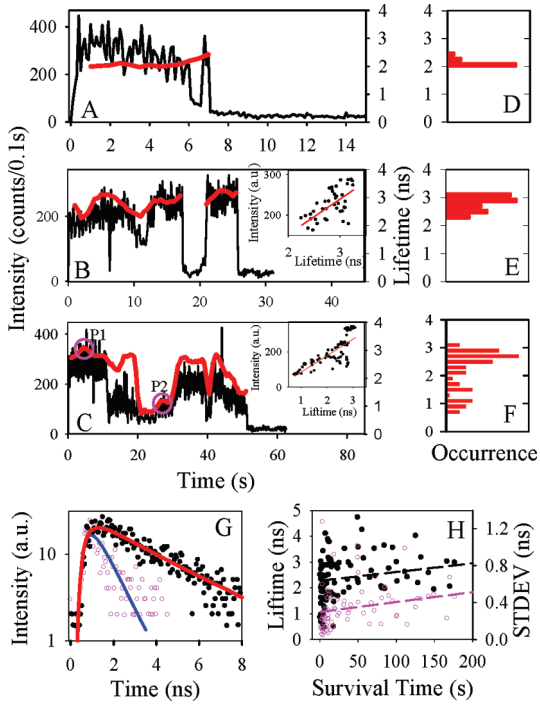

Figure 10. Typical fluorescence intensity (black) and lifetime time (red) trajectories of three single molecules of SRhB−silane on SnO_2 (A−C) and their corresponding lifetime histograms (D−F). The insets in (B) and (C) show the fluorescence intensity as a function of lifetime for these molecules. The fluorescence decays and their single exponential fits of selected points P1 (black circles) and P2 (red circles) in trajectory (C) are shown in (G). The average lifetimes (black filled circles) and standard deviations (pink open circiles) of single molecules as a function of survival times are shown in (H).

which photobleached after 2−3 s. Shown in Figure 10 are examples of a few typical molecules. Compared to ZrO_2, the trajectories of single molecules on SnO_2 show different characteristics due to the presence of the IET pathway. The following are the main differences.

(1) Shorter lifetime and broader distribution: As shown in Figure 9B, the average lifetime on SnO_2 shows a peak centered at ∼2.6 ns and a broad distribution from 600 ps to 4 ns. The total histogram of lifetimes on SnO_2 (Figure 9F) shows Gaussian distributions with center and fwhm of ∼2.6 and 1.5 ns. The peak position is shifted to shorter lifetimes and width is much broader compared to those on ZrO_2. A shorter average single molecule fluorescence lifetime of SRhB−silane on SnO_2 can be attributed to the presence of IET activity, consistent with the observations of ensemble averaged measurements. A broadened distribution of lifetimes on SnO_2 suggests additional broadening due to the distribution of IET rates.

(2) Larger fluctuation of lifetimes within each trajectory. Approximately 60% of single molecule trajectories show small fluctuation of lifetimes ($\sigma < 0.4$ ns), similar to those on ZrO_2. The remaining 40% of molecules show larger fluctuations ($\sigma > 0.4$ ns). Furthermore, in these trajectories lifetime decrease is accompanied by a decrease in fluorescence intensity. This correlation indicates that the lifetime fluctuation is caused by changes in nonradiative decay rates. Among these highly fluctuating molecules, single molecule lifetime histograms are broad, as shown in Figure 10C. In some of these molecules, their lifetimes can change over 2 ns over the duration of the trajectory. The larger fluctuation of lifetimes can be attributed to the fluctuation of IET rates in these donor−bridge−acceptor complexes. An increase in IET rate should reduce the fluorescence lifetime and quantum yield, accounting for the observed correlated lifetime and intensity fluctuations.

(3) Shorter survival time. The survival times of single molecules on SnO_2 are shorter than those on ZrO_2, as shown in Figures 9G,H. The average survival times of single SRhB−silane molecules on ZrO_2 and SnO_2 are 135 and 44 s, respectively. IET to SnO_2 generates oxidized SRhB radical, which is less stable than the ground state molecules and is responsible for the shorter survival time of single molecules on SnO_2. In molecules with shorter survival time, their average fluorescence lifetimes appear to be shorter and their fluctuations (as measured by standard deviation) appear to be smaller, as shown in Figure 10H. It is unclear whether the limited survival time in these trajectories has prevented the sampling of their fluctuations.

ET rate is determined by the electronic coupling between the excited state of the dye molecule and the semiconductor conduction band, driving force, total reorganization energy, and density of states of semicondcutor.[88,89] Distribution of reorganization energy was reported in a previous study of Raman spectrum of single TiO_2 particles sensitized by dye molecules.[90] In addition, static and dynamic heterogeneity of the driving force and electronic coupling strength can also lead to the observed distribution and fluctuation of ET rates. The driving force is determined by the energy of accepting states in the semiconductor and the excited state oxidation potential of the dye molecule. The former is dependent on conduction band edge position, which has been shown to be sensitive to surface charge, such as protonation state.[91,92] Single molecule spectral diffusion has been observed, suggesting possible fluctuations of the excited state oxidation potential of the dye.[85,86] The electronic coupling is strongly dependent on the molecule−substrate interaction, which is likely dependent on the adsorption sites. In the donor−bridge−acceptor system, ET from SRhB to SnO_2 can occur either through superexchange via the silane bridge units or through space. For both pathways, the coupling strength is sensitive to the conformation of the donor−bridge−acceptor complex. To provide further insight into the observed fluctuating single molecule IET dynamics, we have also carried out computational modeling of single SRhB−silane−SnO_2 donor−bridge−acceptor complexes.

Computational Results. Figure 11 shows the ensemble distribution of angles θ_e and adsorbate−surface separations, measured as the distance from the adsorbate center of mass to the semiconductor surface, obtained for an ensemble of configurations generated by MD simulations of SRhB−silane anchored to the SnO_2(110) surface. Figure 11 shows that the distribution of angles is peaked at ∼140 ± 20°, indicating that the orientation of the adsorbate with sulfonate group pointing toward the semiconductor surface remains quite constrained for a wide range of configurations. The broad distribution of adsorbate−surface separations in the 4−18 Å range, indicates that even with a relatively constrained orientation the flexibility of the aminosilane linker allows the linker to get partially solvated and separate from the surface. Most of the underlying broadening is due to the partial solvation of the adsorbate on the hydrated SnO_2 surface and is not observed in analogous MD simulations of SRhB−silane attached to dry SnO_2, where the dominant interactions force SRhB−silane to remain in close contact with the SnO_2 surface.

Figure 12 shows the computed distribution of IET times, τ_{ET}, obtained from an ensemble of 50 000 configurations of the SRhB−silane−SnO_2 system at room temperature, sampled from 100 independent MD trajectories for 1 ns. Figure 12 shows that the distribution of electron injection times is broad with an

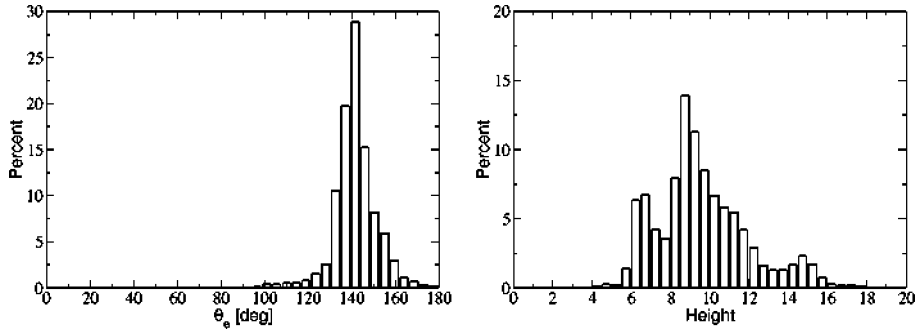

Figure 11. (Left) Distributions of angles between the transition dipole moment of SRhB−silane and the SnO_2 surface normal. (Right) Distribution of adsorbate (center of mass)-surface, separation measured in Å.

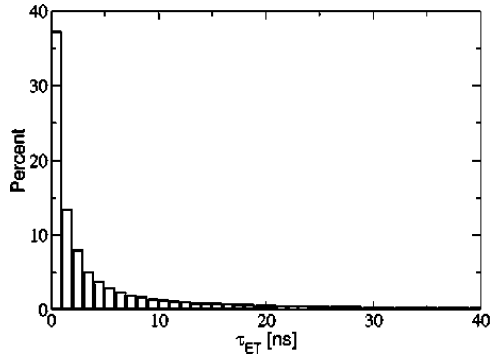

Figure 12. Distribution of IET times obtained as described in the text for an ensemble of 50 000 configurations of the SRhB−silane(H_2O)n−SnO_2 supercell, sampled according to room temperature MD simulations.

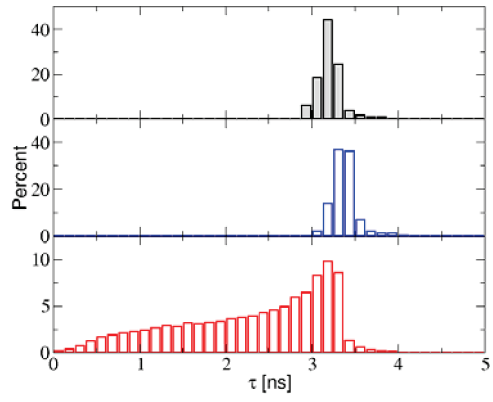

Figure 13. Distributions of intrinsic lifetimes τ (without IET), obtained according to eq 1 for SRhB−silane molecules attached to ZrO_2 (top panel, black) and SnO_2 (middle panel, blue), along with the calculated distribution of observed fluorescence lifetimes τ'(with IET) for SRhB−silane molecules attached to SnO_2 (red).

average injection time of 27.5 ns but with most of the configurations injecting in less than ∼1 ns. The analysis of injection times, as correlated to the orientation and separation of the adsorbate from the surface, indicates that most of the broadening of the distribution shown in Figure 12 is due to the effect of conformational flexibility on the electronic couplings responsible for electron injection.

Figure 13 shows that the distributions of intrinsic fluorescence lifetimes for SRhB−silane on SnO_2 (middle panel) and ZrO_2 (top panel) are quite comparable, centered at ∼3.4 and ∼3.2 ns, respectively. However, due to the effect of IET into SnO_2 (not observed in ZrO_2), the distribution of observed fluorescence lifetimes for SRhB on SnO_2 is shifted by about 1 ns to shorter times (i.e., from ∼3.4 ns to an average fluorescence lifetime of ∼2.3 ns) and broadened when compared to the distribution of total fluorescence lifetimes for SRhB on ZrO_2. These computational results are partially consistent with the experimental observations, reported in Figure 9, where the distribution of lifetimes for SRhB on SnO_2 is broadened and shifted to shorter times (also by ∼1 ns) when compared to the distribution of lifetimes for SRhB on ZrO_2. The simulations, however, predict a broader distribution most likely due to the inherent limitations of the computational method applied for estimations of electron injection times. It should also be noted there are likely distributions of adsorption sites and exposed surfaces on the nanocrystalline films that are studied by the single molecule experiment. These heterogeneities have not been accounted for by the current computational model.

Conclusions

We have investigated the photoinduced interfacial electron transfer process in sulforhodamine B−aminosilane−SnO_2 nanoparticle donor−spacer−acceptor complexes by ensemble average and single molecule spectroscopy. Femtosecond pump−probe transient absorption spectroscopic study shows that in the absence of the spacer ET from SRhB to SnO_2 occurs on the a few picoseconds time scale. In the presence of aminosilane spacer, ET rate from SRhB to SnO_2 is reduced to the nanosecond time scale, which is observed by ensemble average fluorescence lifetime measurement. Wide-field fluorescence images of single SRhB molecules (without spacer) on SnO_2 and glass show that only a smaller number of molecules in the former are observable under single molecule conditions, indicating an incomplete sampling of molecules undergo ultrafast ET on SnO_2. Wide-field images of SRhB−silane−SnO_2 and SRhB−silane−ZrO_2 show similar numbers of observable single molecules. Furthermore, the sum of single molecule decays is shown to be in agreement with the ensemble average fluorescence decay for SRhB−silane−SnO_2. These comparisons suggest a nearly complete sampling of the donor−bridge−acceptor complexes under single molecule conditions.

On the single molecule level, SRhB−silane−ZrO_2 shows a Gaussian distribution of lifetimes with a center a 3.2 ns and a fwhm of 0.9 ns. This is attributed to the distribution of orientation of the molecules relative to surface normal, which leads to variation of radiative decay rates. SRhB−silane−SnO_2 shows a Gaussian distribution of lifetimes with a center a 2.6 ns and a fwhm of 1.5 ns. Shortened lifetime and broadened distribution is attributed to the presence of IET activity in these complexes, which introduces an additional nonradiative decay channel. It is shown that both static distribution and dynamic fluctuation of IET rate are present. Computational modeling of the complexes shows a distribution of molecular conformations, which leads to a distribution of electronic coupling strengths

and ET rates. It is likely that the conversion between these conformations leads to the fluctuation of IET rate and fluorescence lifetime on the single molecule level.

Our study demonstrates that interfacial electron transfer can be studied by single molecule spectroscopy. Single molecule IET studies can determine the distribution of IET rates that underlies the nonsingle exponential kinetics observed in ensemble average measurements. Furthermore, a comparison of single molecule IET study with computational modeling provides detailed insight to the nature of static and dynamic heterogeneity that is difficult to reveal by ensemble average studies alone.

Acknowledgment. V.S.B. acknowledges support from the National Science Foundation (ECCS-0404191), support for preliminary work funded by the Division of Chemical Sciences, Geosciences, and Biosciences, Office of Basic Energy Sciences of the U.S. Department of Energy (DE-FG02-07ER15909), and DOE supercomputer time from the National Energy Research Scientific Center. T.L. is supported the National Science Foundation (CHE-0848556) and the Petroleum Research Fund (PRF No. 49286-ND6).

References and Notes

(1) Miller, R. J. D.; McLendon, G. L.; Nozik, A. J.; Schmickler, W.; Willig, F. *Surface electron transfer processes*; VCH Publishers, Inc.: New York, 1995.
(2) Hagfeldt, A.; Gratzel, M. *Chem. Rev.* **1995**, *95*, 49–68.
(3) Kamat, P. V. *Chem. Rev.* **1993**, *93*, 267–300.
(4) Kamat, P. V. *Prog. React. Kinet.* **1994**, *19*, 277–316.
(5) Kamat, P. V.; Meisel, D. *Semiconductor Nanoclusters - Physical, Chemical, and Catalytic Aspects*; Elsevier: Amsterdam, 1997; Vol. 103.
(6) Anderson, N. A.; Lian, T. *Annu. Rev. Phys. Chem.* **2005**, *56*, 491–519.
(7) O'Regan, B.; Gratzel, M. *Nature* **1991**, *353*, 737–740.
(8) Huynh, W. U.; Dittmer, J. J.; Alivisatos, A. P. *Science* **2002**, *295*, 2425–2427.
(9) Serpone, N. ; Pelizzetti, E. *Photocatalysis, Fundamentals and Applications*; John Wiley & Sons, 1989.
(10) Nitzan, A.; Ratner, M. A. *Science* **2003**, *300*, 1384–1389.
(11) Asbury, J. B.; Hao, E.; Wang, Y.; Ghosh, H. N.; Lian, T. *J. Phys. Chem. B* **2001**, *105*, 4545–4557.
(12) Tachibana, Y.; Moser, J. E.; Graetzel, M.; Klug, D. R.; Durrant, J. R. *J. Phys. Chem.* **1996**, *100*, 20056–20062.
(13) Benko, G.; Myllyperkio, P.; Pan, J.; Yartsev, A. P.; Sundstrom, V. *J. Am. Chem. Soc.* **2003**, *125*, 1118–1119.
(14) Burfeindt, B.; Hannapel, T.; Storck, W.; Willig, F. *J. Phys. Chem.* **1996**, *100*, 16463.
(15) Kuciauskas, D.; Monat, J. E.; Villahermosa, R.; Gray, H. B.; Lewis, N. S.; McCusker, J. K. *J. Phys. Chem. B* **2002**, *106*, 9347–9358.
(16) Piotrowiak, P.; Galoppini, E.; Wei, Q.; Meyer, G. J.; Wiewior, P. *J. Am. Chem. Soc.* **2003**, *125*, 5278–5279.
(17) Bauer, C.; Boschloo, G.; Mukhtar, E.; Hagfeldt, A. *Int. J. Photoenergy* **2002**, *4*, 17–20.
(18) Gaal, D. A.; Hupp, J. T. *J. Am. Chem. Soc.* **2000**, *122*, 10956–10963.
(19) Iwai, S.; Hara, K.; Murata, S.; Katoh, R.; Sugihara, H.; Arakawa, H. *J. Chem. Phys.* **2000**, *113*, 3366–3373.
(20) Rensmo, H.; Keis, K.; Lindstrom, H.; Sodergren, S.; Solbrand, A.; Hagfeldt, A.; Lindquist, S. E.; Wang, L. N.; Muhammed, M. *J. Phys. Chem.* **1997**, *101*, 2598–2601.
(21) Martini, I.; Hodak, J.; Hartland, G. V.; Kamat, P. V. *J. Chem. Phys.* **1997**, *107*, 8064–8072.
(22) Liu, D.; Fessenden, R. W.; Hug, G. L.; Kamat, P. V. *J. Phys. Chem. B* **1997**, *101*, 2583–2590.
(23) Kilsa, K.; Mayo, E. I.; Kuciauskas, D.; Villahermosa, R.; Lewis, N. S.; Winkler, J. R.; Gray, H. B. *J. Phys. Chem. A* **2003**, *107*, 3379–3383.
(24) Hashimoto, K.; Hiramoto, M.; Lever, A. B.; Sakata, T. *J. Phys. Chem.* **1988**, *92*, 1016.
(25) Bedja, I.; Hotchandani, S.; Kamat, P. V. *J. Phys. Chem.* **1994**, *98*, 4133–4140.
(26) Bell, T. D.; Pagba, C.; Myahkostupov, M.; Hofkens, J.; Piotrowiak, P. *J. Phys. Chem. B* **2006**, *110*, 25314–25321.
(27) Rehm, J. M.; McLendon, G. L.; Nagasawa, Y.; Yoshihara, K.; Moser, J.; Gratzel, M. *J. Phys. Chem.* **1996**, *100*, 9577–9578.
(28) Furube, A.; Katoh, R.; Hara, K.; Murata, S.; Arakawa, H.; Tachiya, M. *J. Phys. Chem. B* **2003**, *107*, 4162–4166.
(29) *Single Molecule Spectroscopy: Nobel Conference Lectures*; Rigler, R., Orrit, M., Basche, T., Eds.; Springer: Berlin, 1998.
(30) *Single-Molecule Optical Detection, Imaging and Spectroscopy*; Basche, T., Moerner, W. E., Orrit, M., Wild, U. P., Eds.; VCH: Weinheim, 1997.
(31) Vallee, R. A. L.; Cotlet, M.; Hofkens, J.; De Schryver, F. C.; Muellen, K. *Macromolecules* **2003**, *36*, 7752–7758.
(32) Zhang, L.; Liu, R.; Holman, M. W.; Nguyen, K. T.; Adams, D. M. *J. Am. Chem. Soc.* **2002**, *124*, 10640.
(33) Park, S.-J.; Gesquiere, A. J.; Yu, J.; Barbara, P. F. *J. Am. Chem. Soc.* **2004**, *126*, 4116–4117.
(34) Lu, H. P.; Xie, X. S. *J. Phys. Chem. B* **1997**, *101*, 2753–2757.
(35) Holman, M. W.; Liu, R.; Adams, D. M. *J, Am. Chem. Soc.* **2003**, *125*, 12649–12654.
(36) Goh, W.; Guo, J.; Yuan, R.; Lian, T. In *Proceedings of SPIE-The International Society for Optical Engineering, (Physical Chemistry of Interfaces and Nanomaterials IV)*; Burda, C., Ellingson, R. J., Eds.; 2005; SPIE, Vol. 5929, p 6.
(37) Biju, V.; Micic, M.; Hu, D.; Lu, H. P. *J. Am. Chem. Soc.* **2004**, *126*, 9374–9381.
(38) Yang, H.; Luo, G.; Karnchanaphanurach, P.; Louie, T.-M.; Rech, I.; Cova, S.; Xun, L.; Xie, X. S. *Science (Washington, DC)* **2003**, *302*, 262–266.
(39) Edman, L.; Mets, U.; Rigler, R. *Proc. Natl. Acad. Sci. U.S.A.* **1996**, *93*, 6710–6715.
(40) Wennmalm, S.; Edman, L.; Rigler, R. *Proc. Natl. Acad. Sci. U.S.A.* **1997**, *94*, 10641–10646.
(41) Heinlein, T.; Knemeyer, J.-P.; Piestert, O.; Sauer, M. *J. Phys. Chem. B* **2003**, *107*, 7957–7964.
(42) Sauer, M. *Angew. Chem., Int. Ed.* **2003**, *42*, 1790–1793.
(43) Piestert, O.; Barsch, H.; Buschmann, V.; Heinlein, T.; Knemeyer, J.-P.; Weston, K. D.; Sauer, M. *Nano Lett.* **2003**, *3*, 979–982.
(44) Neuweiler, H.; Schulz, A.; Boehmer, M.; Enderlein, J.; Sauer, M. *J. Am. Chem. Soc.* **2003**, *125*, 5324–5330.
(45) Huang, J.; Stockwell, D.; Boulesbaa, A.; Guo, J.; Lian, T. *J. Phys. Chem. C* **2008**, *112*, 5203–5212.
(46) Ghosh, H. N.; Asbury, J. B.; Lian, T. *J. Phys. Chem. B* **1998**, *102*, 6482–6486.
(47) Tachibana, Y.; Haque, S. A.; Mercer, I. P.; Durrant, J. R.; Klug, D. R. *J. Phys. Chem. B* **2000**, *104*, 1198–1205.
(48) Kitamura, T.; Ikeda, M.; Shigaki, K.; Inoue, T.; Anderson, N. A.; Ai, X.; Lian, T.; Yanagida, S. *Chem. Mater.* **2004**, *16*, 1806–1812.
(49) Palomares, E.; Clifford, J. N.; Haque, S. A.; Lutz, T.; Durrant, J. R. *Chem. Commun.* **2002**, 1464–1465.
(50) Guo, J.; She, C.; Lian, T. *J. Phys. Chem. C* **2007**, *111*, 8979–8987.
(51) Anderson, N. A.; Ai, X.; Chen, D.; Mohler, D. L.; Lian, T. *J. Phys. Chem. B* **2003**, *107*, 14231–14239.
(52) Asbury, J. B.; Hao, E.; Wang, Y.; Lian, T. *J. Phys. Chem. B* **2000**, *104*, 11957–11964.
(53) Galoppini, E. *Coord. Chem. Rev.* **2004**, *248*, 1283–1297.
(54) Durrant, J. R.; Haque, S. A.; Palomares, E. *Coord. Chem. Rev.* **2004**, *248*, 1247–1257.
(55) Cui, X. D.; Primak, A.; Zarate, X.; Tomfohr, J.; Sankey, O. F.; Moore, A. L.; Moore, T. A.; Gust, D.; Harris, G.; Lindsay, S. M. *Science* **2001**, *294*, 571–574.
(56) Karstens, T.; Kobs, K. *J. Phys. Chem.* **1980**, *84*, 1871–1872.
(57) Huang, J.; Stockwell, D.; Boulesbaa, A.; Guo, J.; Lian, T. *J. Phys. Chem. C* **2007**, *112*, 5203–5212.
(58) Chan, E. W. L.; Yousaf, M. N. *J. Am. Chem. Soc.* **2006**, *128*, 15542–15546.
(59) Rockenberger, J.; zum Felde, U.; Tischer, M.; Troger, L.; Haase, M.; Weller, H. *J. Chem. Phys.* **2000**, *112*, 4296–4304.
(60) Macklin, J. J.; Trautman, J. K.; Harris, T. D.; Brus, L. E. *Science* **1996**, *272*, 255–258.
(61) Lukosz, W.; Kunz, R. E. *Opt. Commun.* **1977**, *20*, 195–199.
(62) *Handbook of Chemistry and Physics*, 77th ed.; Lide, D. R., Ed.; CRC Press: Boca Raton, FL, 1996; p 4-130−4-136.
(63) Becke, A. D. *J. Chem. Phys.* **1993**, *98*, 5648–5652.
(64) Hehre, W. J.; Ditchfie, R.; Pople, J. A. *J. Chem. Phys.* **1972**, *56*, 2257-&.
(65) Harihara, Pc; Pople, J. A. *Theor. Chim. Acta* **1973**, *28*, 213–222.
(66) Bauernschmitt, R.; Ahlrichs, R. *Chem. Phys. Lett.* **1996**, *256*, 454–464.
(67) Casida, M. E.; Jamorski, C.; Casida, K. C.; Salahub, D. R. *J. Chem. Phys.* **1998**, *108*, 4439–4449.
(68) Stratmann, R. E.; Scuseria, G. E.; Frisch, M. J. *J. Chem. Phys.* **1998**, *109*, 8218–8224.
(69) Phillips, J. C.; Braun, R.; Wang, W.; Gumbart, J.; Tajkhorshid, E.; Villa, E.; Chipot, C.; Skeel, R. D.; Kale, L.; Schulten, K. *J. Comput. Chem.* **2005**, *26*, 1781–1802.
(70) She, C.; Guo, J.; Lian, T. *J. Phys. Chem. B* **2007**, *111*, 6903–6912.

(71) Guo, J.; She, C.; Lian, T. *J. Phys. Chem. B* **2005**, *109*, 7095–7102.
(72) Cornell, W. D.; Cieplak, P.; Bayly, C. I.; Gould, I. R.; Merz, K. M.; Ferguson, D. M.; Spellmeyer, D. C.; Fox, T.; Caldwell, J. W.; Kollman, P. A. *J. Am. Chem. Soc.* **1995**, *117*, 5179–5197.
(73) Bandura, A. V.; Sofo, J. O.; Kubicki, J. D. *J. Phys. Chem. B* **2006**, *110*, 8386–8397.
(74) Kresse, G.; Hafner, J. *Phys. Rev. B* **1993**, *47*, 558–561.
(75) Kresse, G.; Furthmuller, J. *Comput. Mater. Sci.* **1996**, *6*, 15–50.
(76) Kresse, G.; Furthmuller, J. *Phys. Rev. B* **1996**, *54*, 11169–11186.
(77) Vanderbilt, D. *Phys. Rev. B* **1990**, *41*, 7892–7895.
(78) Wang, Y.; Perdew, J. P. *Phys. Rev. B* **1991**, *44*, 13298–13307.
(79) Li, J. R.; Nilsing, M.; Kondov, I.; Wang, H. B.; Persson, P.; Lunell, S.; Thoss, M. *J. Phys. Chem. C* **2008**, *112*, 12326–12333.
(80) Cerda, J.; Soria, F. *Phys. Rev. B* **2000**, *61*, 7965–7971.
(81) Newton, M. D. *Chem. Rev.* **1991**, *91*, 767–792.
(82) Grabowski, Z. R.; Rotkiewicz, K. *Chem. Rev.* **2003**, *103*, 3899.
(83) Magde, D.; Rojas, G. E.; Seybold, P. G. *Photochem. Photobiol.* **1999**, *70*, 737.
(84) Lukosz, W.; Kunz, R. E. *Opt. Commun.* **1977**, *20*, 195–199.
(85) English, D. S.; Harbron, E. J.; Barbara, P. F. *J. Chem. Phys.* **2001**, *114*, 10479–10485.
(86) Xie, X. S. *Acc. Chem. Res.* **1996**, *29*, 598–606.
(87) Xie, X. S.; Trautman, J. K. *Annu. Rev. Phys. Chem.* **1998**, *49*, 441–480.
(88) Marcus, R. A. *J. Chem. Phys.* **1956**, *24*, 966–978.
(89) Marcus, R. A. *Annu. Rev. Phys. Chem.* **1964**, *15*, 155–196.
(90) Pan, D.; Hu, D.; Lu, H. P. *J. Phys. Chem. B* **2005**, *109*, 16390–16395.
(91) She, C.; Anderson, N. A.; Guo, J.; Liu, F.; Goh, W.; Chen, D.-T.; Mohler, D. L.; Tian, Z.-Q.; Hupp, J.; Lian, T. *J. Phys. Chem. B.* **2005**, *109*, 19345–55.
(92) Boschloo, G.; Fitzmaurice, D. *J. Phys. Chem. B* **1999**, *103*, 3093–3098.

JP911662G